PEM Electrolysis-Assisted Catalysis Combined with Photocatalytic Oxidation towards Complete Abatement of Nitrogen-Containing Contaminants in Water

Ampurdanés, Jordi; Bunea, Sorin; Urakawa, Atsushi

DOI
10.1002/cssc.202002828

Publication date
2020

Document Version
Final published version

Published in
ChemSusChem

Chemistry Europe
European Chemical Societies Publishing

PEM Electrolysis-Assisted Catalysis Combined with Photocatalytic Oxidation towards Complete Abatement of Nitrogen-Containing Contaminants in Water

Jordi Ampurdanés,[a] Sorin Bunea,[b] and Atsushi Urakawa*[a, b]

Electrolysis-assisted nitrate (NO_3^-) reduction is a promising approach for its conversion to harmless N_2 from waste, ground, and drinking water due to the possible process simplicity by in-situ generation of H_2/H/H^+ by water electrolysis and to the flexibility given by tunable redox potential of electrodes. This work explores the use of a polymer electrolyte membrane (PEM) electrochemical cell for electrolysis-assisted nitrate reduction using SnO_2-supported metals as the active cathode catalysts. Effects of operation modes and catalyst materials on nitrate conversion and product selectivity were studied. The major challenge of product selectivity, namely complete suppression of nitrite (NO_2^-) and ammonium (NH_4^+) ion formation, was tackled by combining with simultaneous photocatalytic oxidation to drive the overall reaction towards N_2 formation.

Introduction

The intensive use of fertilizers in agriculture, triggered by the invention of the Haber-Bosch process at the beginning of twentieth century, is the most important cause of the anthropogenic perturbation of Earth's reactive nitrogen cycle.[1] Nitrate leaching in ground water represents a major environmental problem, leading to appearance of hypoxic areas both in oceans and fresh water bodies, known as dead zones. Furthermore, the presence of nitrate in drinking water can cause serious health conditions, such as methemoglobinemia, as well as reproductive problems and cancer.[1]

The Council of Europe (CoE) and the United States Environmental Protection Agency (EPA) have established the maximum admissible concentration for nitrate ions in drinking water to 50 and 45 mg L^{-1}, respectively, in accordance with the guideline defined by the World Health Organization (WHO).[2–4] The maximum allowed concentrations for nitrite (NO_2^-) and ammonium (NH_4^+) ions in drinking water, established by CoE, are 0.5 mg L^{-1} for both ions.[5] The regulations for these ions are stricter by an order of magnitude than that for nitrate ions, stressing the higher risks of these nitrate derivatives pose for human health when present in drinking water. Therefore, development and application of treatment technologies to remove NO_3^- from groundwater, while minimizing formation of other nitrogen-containing compounds and ions, is of utmost importance. There are various technologies available for nitrate removal such as ion exchange, reverse osmosis, electrodialysis, and biological/chemical denitrification.[6] Separation-based methods are well established, but at the same time highly concentrated nitrate solutions are obtained as by-product. In this light, the most attractive and desired strategy is to convert nitrate ions to harmless gaseous nitrogen.

Catalytic hydrogenation of nitrate ions has been considered as one of the most effective methods for their abatement and has been widely investigated over the past three decades.[7–12] One practical challenge is related to the infrastructure for usage and storage of hydrogen gas. Another great challenge is the frequently reported poor N_2 selectivity, as nitrite and ammonium ions, often formed as side-products, are more harmful and undesired than nitrate ions.[13]

In parallel to the development of catalytic nitrate reduction technologies, electrocatalytic removal of nitrates has gained attention in the last decades and embraces a large part of the electrochemistry of nitrogen-containing compounds.[14] Possible reaction pathways for nitrate and nitrite reduction on various electrodes have been described in detail in the literature.[15–20] In this context, combining the reduction of nitrate ions by electrochemically produced hydrogen from water, powered by renewable energies, is attractive since both processes can be performed simultaneously without a need of external H_2 source, such as producing green H_2 on demand from water.

Hasnat et al. reported selective electrocatalytic hydrogenation of NO_3^- to N_2 and NH_3 in a batch electrochemical cell with different metals as active cathode catalysts, including copper,

[a] Dr. J. Ampurdanés, Prof. A. Urakawa
Institute of Chemical Research of Catalonia (ICIQ)
Barcelona Institute of Science and Technology (BIST)
Avinguda Països Catalans 16, 43007 Tarragona (Spain)
[b] S. Bunea, Prof. A. Urakawa
Catalysis Engineering, Department of Chemical Engineering
Delft University of Technology
Van der Maasweg 9, 2629HZ Delft (The Netherlands)
E-mail: A.Urakawa@tudelft.nl

Supporting information for this article is available on the WWW under https://doi.org/10.1002/cssc.202002828

This publication is part of a Special Collection highlighting "The Latest Research from our Board Members". Please visit chemsuschem.org/collections to view all contributions.

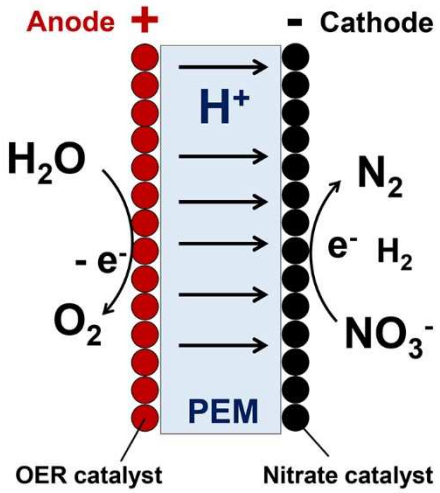

Figure 1. Electrolysis-assisted concept for continuous nitrate (electro) catalytic hydrogenation using the PEM technology, with oxygen evolution reaction (OER) taking place at the anode of the cell.

tin, silver, palladium, and platinum.[21–25] The use of a Nafion® (hereafter denoted as "Nafion") proton exchange membrane allowed the transport of protons generated in situ at the anode side to the surface of the catalyst deposited at the cathode side, enabling nitrate reduction as illustrated in Figure 1. Recently, such a combined approach is gaining increasing attention in the scientific community.[26–31]

The batch mode of operation may restrict its potential industrial application due to the limited volume of processible solutions as well as high operational costs. An obvious and more practical approach is to perform the electrocatalytic nitrate reduction in a continuous mode. Besides, by using a proton exchange membrane (PEM) system, the reduction activity may be boosted due to the enhanced H_2/H^+ concentrations locally at the interface (cathode catalyst surface) and to the electrical potential tunable at will. Nevertheless, the evaluation of the approach for nitrate reduction requires deeper and systematic investigations. The aim of this work is to evaluate the potential of the combined approach, termed here as electrolysis-assisted nitrate reduction process, for wastewater (here synthetic solution) purification meeting the international legislation limits for drinking water quality. Monometallic and bimetallic nanoparticles of Pt, Pd, Cu, and PdCu, known to show good to excellent nitrate hydrogenation activity in thermal catalysis, were supported on high-surface-area tin oxide (SnO_2) and used as cathode catalysts for electrolysis-assisted nitrate reduction in a continuous as well as batch mode of operation.[13] The optimum strategy for selective NO_3^- reduction to molecular nitrogen was sought by using several modes of operation. Furthermore, a new effective strategy is reported to solve the problem of product selectivity by combining the electrolysis-assisted approach with a photocatalytic oxidation route to maximize N_2 selectivity.

Results and Discussion

Electrolysis-assisted nitrate reduction

The continuous electrolysis-assisted nitrate reduction configuration employed for testing is shown in Figure 2A. The cell previously employed for water electrolysis was used for this study.[32,33] As shown in Figure 3, several operational modes or flow conditions were evaluated using the same electrochemical cell without making any modification to the membrane electrode assemblies (MEAs). These are: (i) potential sweep (potentiodynamic) conditions (Figure 3a), gradually (step-wise) increasing cell voltage with time; (ii) constant potential mode (Figure 3b); and (iii) constant current (galvanostatic) mode (Figure 3c). In all cases, one-pass flow-through condition was used. Regarding flow conditions, we evaluated a flow-through operation in a loop mode by recirculating the effluent solution back to the cathode compartment (Figure 3d). Furthermore, ex situ (i.e., not generated in the PEM cell) hydrogen was directly bubbled at the inlet of the cathode compartment (leading to a H_2-saturated solution) without applying cell voltage (Figure 3e). This mode allows examining catalytic hydrogenation activity of the catalysts coated over the Nafion membrane.

Among all operational modes shown in Figure 3, the most efficient one to evaluate different catalysts is the potential sweep mode, since it readily indicates the effect of cell potential on the reaction performance. This mode was used to clarify the trends of electrocatalytic activity and product selectivity of the monometallic and bimetallic catalysts.

Continuous-flow tests

The continuous electrolysis-assisted nitrate reduction (Figure 2A) was first evaluated by potential sweep measurements by gradually increasing the PEM cell voltage in a step-wise fashion (from 1.5 to 2.7 V, $\Delta V = 0.2$ V, 60 min each step, Figure 3a). A 100 ppm aqueous nitrate solution was fed through the cathode compartment at a constant flow rate of 160 $\mu L\,min^{-1}$. The reaction performance of MEAs consisting of IrO_2 | Nafion | 40 wt% M/SnO_2 (anode catalyst | PEM | cathode catalyst, M=Pt, Pd, Cu, and PdCu), as well as that of an MEA using the bare support (SnO_2) as cathode catalyst were evaluated.

The product quantification indicated that nitrate removal took place over all materials evaluated (Figure 4a). Generally, higher nitrate conversion was observed at higher cell voltage. This suggests electrocatalytic promotion for nitrate reduction or enhanced hydrogenation activity due to higher surface hydrogen concentration at the cathode catalyst surface. The bare SnO_2 consistently gave the lowest nitrate conversions among all the materials examined at all cell voltages and the addition of metal(s) to the SnO_2 support prominently enhanced the nitrate conversion. The PdCu catalyst was clearly the best one, reaching almost full nitrate conversion [herein referred as $X(NO_3^-)$], approximately 95% at 2.7 V, followed by Pt (≈85%) and Pd catalysts (≈80%). The Cu catalyst showed the poorest $X(NO_3^-)$

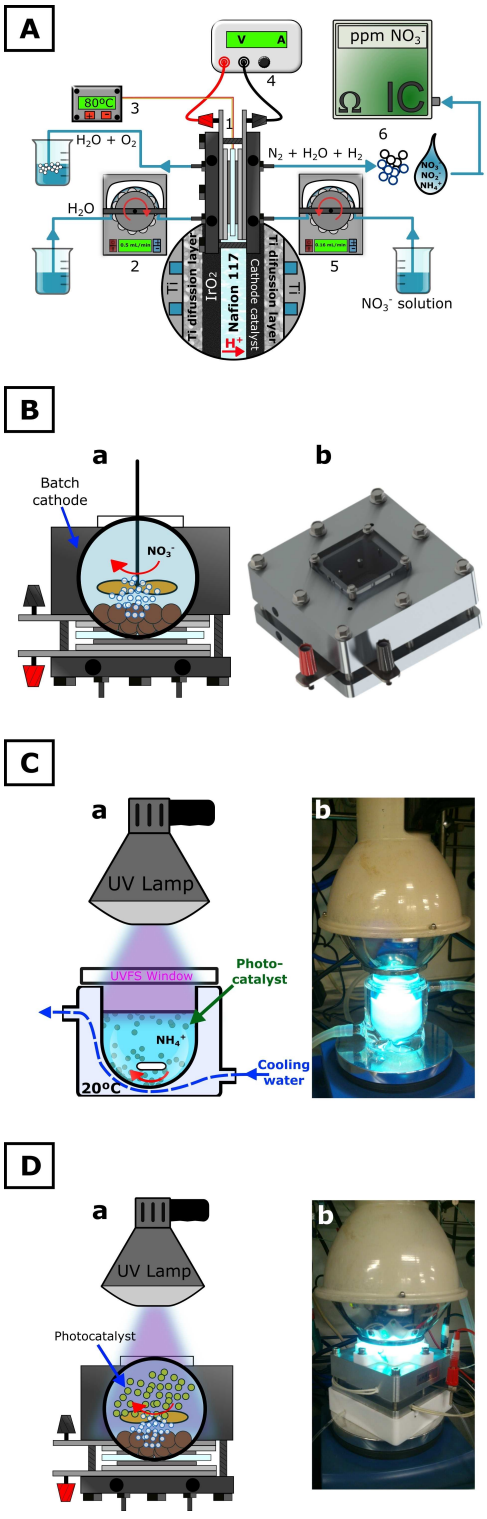

Figure 2. Strategies for NO_3^- reduction and NH_4^+ mitigation evaluated in this work. (A) Continuous electrocatalytic reaction for electrolysis-assisted nitrate hydrogenation where (1) PEM cell, (2) peristaltic pump and water reservoir, (3) temperature controller, (4) computer controlled potentiostat, (5) peristaltic pump and nitrate solution reservoir, and (6) ion chromatograph for product analysis. (B) Batch mode of operation using the same cell by replacing the housing for the cathode compartment with a 20 mL aluminum reservoir. (a) Schematic side view and (b) the assembled cell. (C) Batch reactor used for photocatalytic ammonium ion oxidation. (a) Schematic representation and (b) the lab system in action. (D) Combined operation of electrolysis-assisted hydrogenation and photocatalytic oxidation using the batch cell. (a) Schematic representation and (b) the lab system in action.

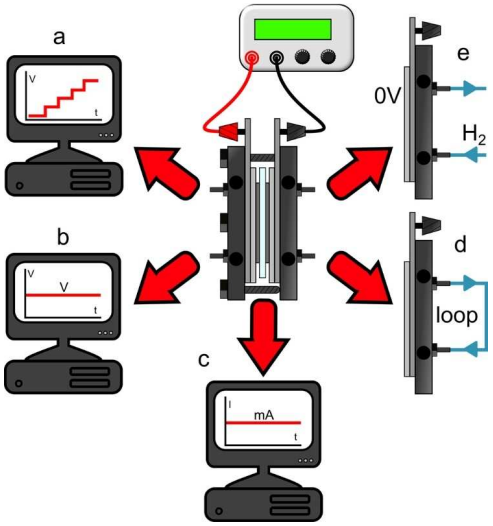

Figure 3. Various modes of operation for NO_3^- reduction performed in this work using the identical cell: (a) potential sweep mode with step-wise cell voltage increase, (b) constant potential mode, (c) constant current mode, (d) recirculation mode at constant current of 100 mA, and (e) catalytic reduction at 0 V using hydrogen-saturated nitrate solution.

(≈65%) among the supported metal catalysts, although its activity improved at higher cell potential without any sign of deactivation, which could indicate the dominance of catalytic hydrogenation at these conditions. It is also remarkable that for the best catalyst (PdCu), at an intermediate potential of 2.1 V, nitrate conversion value already reached approximately 80%.

Differentiating whether nitrate reduction proceeds via electrolysis-assisted hydrogenation or via electrochemical reduction is not a straightforward task when the reaction is conducted in a PEM cell, as a reference electrode is not available and the implementation of spectroscopic techniques for mechanistic studies is challenging. Machida et al. investigated the change in pH of the nitrate solution undergoing reduction in the PEM to find an answer to this question.[21] The hydrogenation pathway is accompanied by pH increase, following Equation (1).

$$2NO_3^- + 5H_2 \rightarrow N_2 + 2OH^- + 4H_2O \quad (1)$$

In the electrochemical pathway, two reactions can take place, Equation (2) and Equation (3), of which only Equation (3) is accompanied by pH increase.

$$2NO_3^- + 12H^+ + 10e^- \rightarrow N_2 + 6H_2O \quad (2)$$

$$2NO_3^- + 6H_2O + 10e^- \rightarrow N_2 + 12OH^- \quad (3)$$

For PdCu, an increase in pH with increasing cell voltage was observed from 1.5 to 2.1 V, since OH^- is formed during NO_3^- reduction. The pH was almost constant in the 2.1 to 2.7 V cell potential range. At the end of the potential sweep (2.7 V), the pH value was about 11. These values are consistent with theoretical ones expected for the catalytic nitrate hydrogena-

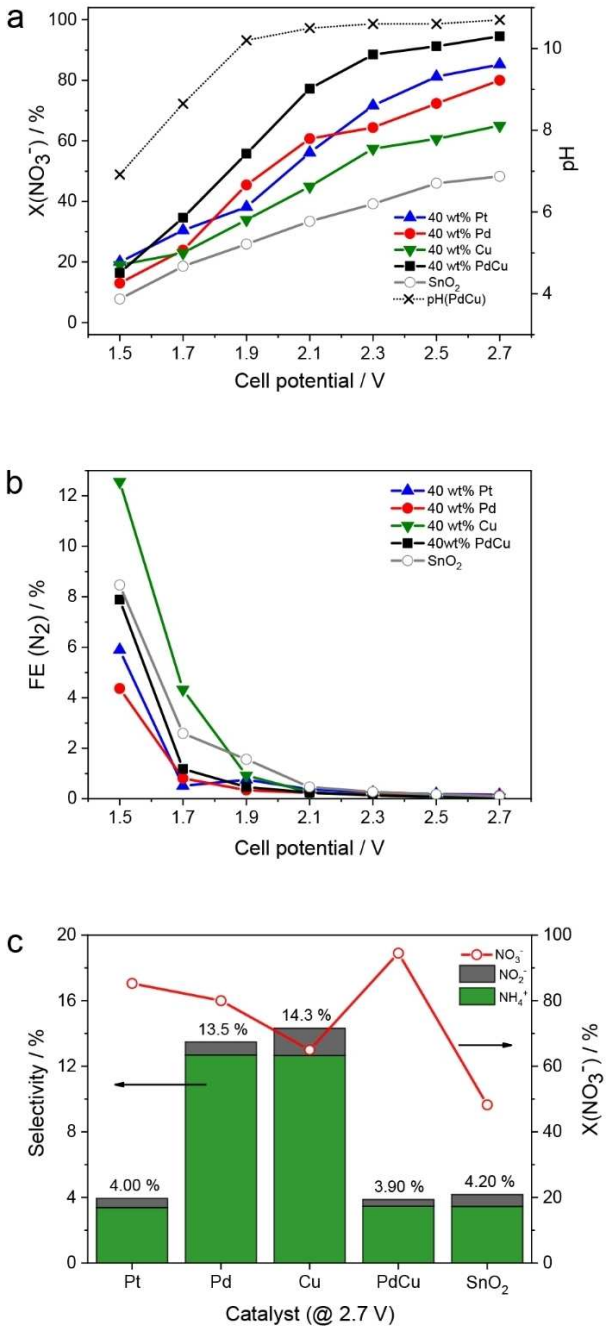

Figure 4. Potential sweep study. (a) Nitrate conversion profiles over 7 h of potential sweep experiments (from 1.5 to 2.7 V, $\Delta V = 0.2$ V, 60 min each step) of electrolysis-assisted nitrate reduction. Four different catalysts: Pt, Pd, Cu, PdCu, and bare SnO_2 were tested at 80 °C with nitrate solution of 100 ppm NO_3^- at 160 µL min^{-1}. Electro-osmotic drag effect was corrected; pH profile during electrolysis-assisted nitrate reduction over 7 h of potential sweep experiment; electro-osmotic drag effect corrected. (b) Faradaic efficiency towards nitrogen formation $FE(N_2)$ as a function of cell potential for the four investigated catalysts. (c) $X(NO_3^-)$, $S(NO_2^-)$ and $S(NH_4^+)$, at 2.7 V for all catalysts and bare support.

tion pathway [Eq. (1)].[21] In case of a pure electrochemical reaction [Eq. (2)], the expected theoretical pH is around 12.

We estimated the faradaic efficiency [$FE(N_2)$] for nitrogen formation (Figure 4b) of the studied catalysts. The highest FE was observed for Cu, 13% at 1.5 V cell potential. In general, for all the investigated materials, the highest $FE(N_2)$ was observed at 1.5 V cell potential. Nevertheless, $FE(N_2)$ decreased drastically with increasing cell potential. At cell potential between 2.1 and 2.7 V, $FE(N_2)$ fell to <1%. Although it is tempting to correlate the higher $FE(N_2)$ values at low cell potentials to the dominance of the electrochemical pathway in nitrate reduction [Eq. (2)], this hypothesis is not supported by the pH increase that was observed during experiments. Furthermore, the faradaic efficiency does not provide information regarding the underlying reaction mechanism and only indicates to which extent the supplied electrons are used for the formation of the desired reaction product. The reason for higher $FE(N_2)$ values at low cell potentials is likely due to the low amount of evolved hydrogen at these reaction conditions, which leads to an almost stoichiometric ratio of nitrates and hydrogen. In this way, a higher $FE(N_2)$ is obtained from calculations. Considering the low $FE(N_2)$ at high cell potentials, caused by a high rate of hydrogen evolution, it can be concluded that the dominating pathway of nitrate conversion to nitrogen in the PEM cell is the electrolysis-assisted hydrogenation pathway [Eq. (1)].

Generally, nitrite selectivity, $S(NO_2^-)$, was low for all the tested catalysts. Still, upon cell potential increase, an increase in $S(NO_2^-)$ was observed in the cell potential range between 1.5–2.1 V, followed by a noticeable decrease of $S(NO_2^-)$ at 2.7 V cell potential (Figure 4c, the results between 1.5–2.5 V not shown). The selectivity to another undesired product, ammonium, $S(NH_4^+)$ increased with increasing cell voltages for Pd and Cu catalysts, whereas for PdCu, Pt, and SnO_2 the tendency was opposite (results not shown). PdCu, which gave the highest $X(NO_3^-)$, also gave the best results in terms of N_2 selectivity, judging from the low selectivity to side products [$S(NO_2^-) + S(NH_4^+) \approx 3.9$% at 2.7 V, Figure 4c] throughout the investigated cell potential range. In the analysis of evolved gaseous species by online mass spectrometry (MS), we did not observe the formation of gaseous side-products (i.e., N_2O, NO, NH_3, or NH_2OH).

The Pt catalyst exhibited similarly good results in terms of selectivity towards nitrogen [$S(NO_2^-) + S(NH_4^+) \approx 4$%]. Hence, both PdCu and Pt can offer high nitrogen selectivity [$S(N_2)$] of around 96% (Figure 4c). Judging from both $X(NO_3^-)$ and $S(i)$ ($i = NO_2^-$, NH_4^+, N_2) the best-performing catalyst for electrolysis-assisted nitrate reduction is concluded to be 40 wt% PdCu/SnO_2 (Figure 4c). This catalyst gives almost full conversion of nitrates and high selectivity towards N_2, albeit relatively high cell potentials were required to achieve this remarkable performance. We selected this material as a reference cathode catalyst for further investigations to evaluate the effects of different cell operation modes on the reaction performance.

Furthermore, the stability of MEA containing the PdCu catalyst during long term operation (46 h) was investigated at a relatively harsh high potential (2.8 V) condition (Supporting Information, Figure S1). A stable nitrate conversion (>85%) was observed over the period with relatively high selectivity to NH_4^+. XRD patterns of the catalyst in the MEA before and after the potential sweep operation (Supporting Information, Figure S2) show no notable changes in the crystal structure of the

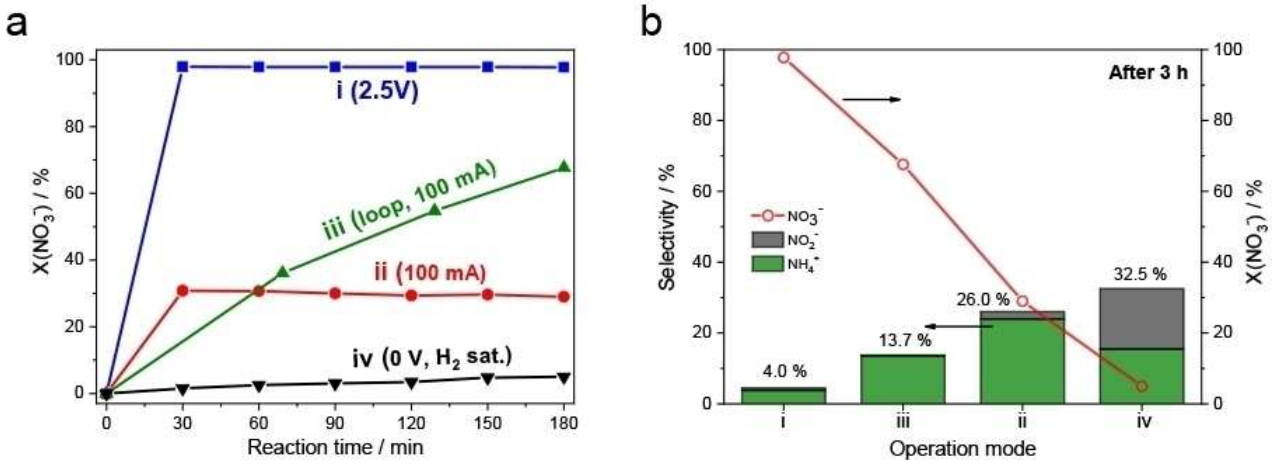

Figure 5. (a) Evaluation of different operational modes in electrolysis-assisted nitrate reduction using 40 wt% PdCu/SnO_2 as the cathode catalyst at 80 °C with 100 ppm nitrate solution for 3 h. Freshly prepared MEA was used for each measurement. Operational modes: (i) constant cell voltage mode at 2.5 V; (ii) constant current mode at 100 mA, (iii) recirculation mode at constant current of 100 mA, and (iv) catalytic nitrate hydrogenation over the MEA without applying cell voltage. The flow rate of the nitrate solution was 160 μL min^{-1}. (b) $X(NO_3^-)$ and undesired product selectivity [$S(NO_2^-)$ and $S(NH_4^+)$], after 3 h, obtained for the four operational modes. The values shown on top of the bars are total selectivity to the undesired products.

catalysts, indicating good stability of the PdCu and SnO_2 under the electrolysis condition.

System flexibility evaluation

The results described above in the continuous operation mode are comparable with the best results reported by Machida et al., where a pH buffering agent (CO_2) was used.[21] Encouraged by the results, we extended our study to further minimize the selectivity towards undesired reaction products and improve the reaction performance. It has to be highlighted that although the selectivity towards undesired products is relatively low (≈4%), one should mind the more stringent regulations for NO_2^- (0.5 ppm) and NH_4^+ (0.5 ppm) compared to NO_3^- (50 ppm) in drinking water (98/83/EC). This means that $S(NH_4^+)$ + $S(NO_2^-)$ should be lower than approximately 2.5%, if their amounts are almost the same. To tackle this great challenge, different operation modes, as well as system configurations, were tested as follows:

(i) Constant cell voltage operation mode (Figure 3b). The electrolysis-assisted nitrate reduction at high cell potential (2.5 V) was examined during 3 h time, based on the excellent performance observed for the PdCu catalyst at this cell potential (Figure 4).

(ii) Constant-current operation mode (Figure 3c). The advantage of this operation mode is the mitigation of fluctuations in H^+ transport through the Nafion membrane, and therefore in hydrogen production rate at the cathode. The chosen constant current value was relatively low, to avoid affecting the membrane stability. Other reaction conditions remained unchanged (temperature, solution flow rate, cathode and anode catalyst composition). A freshly prepared membrane was used and the applied electric current was fixed at 100 mA (6.25 mA cm^{-2}), giving an average cell potential value of 1.6 V, that is, in the low cell potential region.

(iii) "Loop" (i.e., recirculation) operation mode (Figure 3d). The effluent solution was recirculated through the nitrate solution/effluent reservoir (C_0 = 100 ppm, 10 mL) by means of a peristaltic pump. In this operation mode, the improvement of the reaction performance was aimed by increasing the residence time of the nitrate solution in the cell, and hence the contact time of reacting ions with the catalyst surface. With the chosen solution flow rate and the volume of the reservoir, the solution has passed through the cell approximately three times in 3 h. In this operation mode, a constant current of 100 mA (6.25 mA cm^{-2}) was applied to the cell. The average recorded cell potential was 1.6 V.

(iv) Catalytic nitrate hydrogenation by the PdCu catalyst coated over the Nafion membrane (Figure 3e). The reaction was performed at 80 °C by saturating the nitrate solution with H_2 before it entered the cell. In this case, no voltage (0 V) was applied to the cell. The flow rate of the H_2-saturated nitrate solution was kept the same as in previous experiments (160 μL min^{-1}).

Figure 5a shows the $X(NO_3^-)$ profiles along 3 h of continuous operation using the four different strategies described above. The continuous flow electrocatalytic reduction at 2.5 V (blue line) showed the best results in terms of nitrate conversion (≈97%) and stability after a short activation time of 30 min. The second strategy, constant current mode operation at 100 mA (6.25 mA cm^{-2}), did not show a satisfactory performance with nitrate conversion reaching only approximately 30%, and exhibiting a slight decrease in activity over time (red line). In contrast, by increasing the contact time of the solution with the catalyst using the recirculation strategy at 100 mA (6.25 mA cm^{-2}), the reaction performance was clearly improved (green line). After 3 h, $X(NO_3^-)$ of approximately 68% was

achieved. Importantly, the conversion increased linearly with time and 84% nitrate conversion could be attained after 4 h (not shown). This is an important finding since this strategy clearly shows that the reaction performance can be improved even under mild conditions (low cell voltages) by changing the operation mode and conditions. The catalytic nitrate hydrogenation mode (0 V), in which a H_2-saturated NO_3^- solution was supplied to the cathode, exhibited a negligible conversion ($\approx$5%, Figure 5a, black line), showing that the hydrogen dissolved in water cannot be efficiently activated over the catalyst to reduce nitrates. A reason for the low performance could be the low solubility of hydrogen in water (1.62 mg kg^{-1} at 293.15 K and 10^5 Pa gas pressure) and the consequent arising mass transfer limitations at the catalyst surface.[34] Based on these results, it can be concluded that the electrochemically-generated hydrogen/protons at the cathode surface are crucial for achieving high nitrate reduction performance in the PEM cell. The enhanced hydrogenation activity may originate from an electrochemical promotion effect known as NEMCA (non-daradaic electrochemical modification of catalytic activity) effect or EPOC (electrochemical promotion of catalysis), although the origin of the activity enhancement has not been firmly identified in this work.[35–37]

The reaction performance cannot be evaluated solely by the nitrate conversion value. The reaction selectivity after 3 h of reaction is graphically summarized in Figure 5b. Interestingly, a clear trend between product selectivity and conversion could be established: the higher the nitrate conversion, the lower the selectivity towards the undesired products. The constant potential operation mode (i) afforded the highest conversion of nitrates ($\approx$97%) and highest selectivity to N_2. The second-best strategy was the recirculation mode at (iii) with the selectivity towards the undesired products of 13.7% and $X(NO_3^-)$ of 68%. The third best performing operation mode was the constant current mode (100 mA, 6.25 mA cm^{-2}) without recirculation (ii), exhibiting a selectivity towards undesired products of ca. 26% and $X(NO_3^-)$ of 29%. Finally, the worst performing strategy in terms of reaction selectivity was the catalytic hydrogenation in the PEM cell with external hydrogen supply (iv), with a notably high selectivity to undesired products of 32.5% and low $X(NO_3^-)$ of 5%. The detailed evaluation of system flexibility and different operation modes provided us interesting and useful insights for achieving the best possible nitrate reduction performance to nitrogen using the PEM cell. The excellent performance of electrolysis-assisted hydrogenation in terms of high N_2 selectivity must be highlighted since in traditional catalytic hydrogenation selectivity is the major drawback and challenge.[13]

Advancing NO_3^-/NH_4^+ mitigation strategies

Although the reaction performance was strikingly high in the constant cell voltage mode, lowering the working cell voltage and thus current density would be desired for (i) overall system long-term stability, (ii) lowering electrical energy input for operation and (iii) most importantly, efficient utilization of electrochemically generated hydrogen exclusively for the hydrogenation of nitrates, that is, reaching high FE towards nitrogen. This study already showed that the increase in residence time of the solution in the cathode compartment can proportionally enhance the nitrate conversion. The next step was to examine the operation with longer residence time, and thus the batch operation mode was investigated.[21–23,38]

Low-potential electrolysis-assisted batch operation configuration

The MEA composition (PdCu catalyst) was the same as in previous experiments. A fresh MEA was tested for 3 h at 100 mA (6.25 mA cm^{-2}) applied current. Switching to the batch configuration led to an increase in the cell voltage (1.8 V) compared to the flow-through operation (1.6 V) at constant current. We refer to this approach as electro-batch configuration (Figure 2B). The nitrate conversion and product selectivity profiles are shown in Figure 6. After 3 h of batch operation using the PdCu catalyst, $X(NO_3^-)$ reached approximately 95% (red line), showing very similar high catalytic activity as in the case of the flow system at high cell potential (Figure 5a, blue line). The nitrate conversion increased with time, but very high selectivity to side products [$S(NO_2^-)+S(NH_4^+)$] was observed, decreasing from approximately 98 to 58% (Figure 6, green and grey bars) with reaction time. These selectivity values are more than one order of magnitude higher than those observed in the flow operation mode. The dominating product was ammonium, reaching a stable selectivity value $S(NH_4^+)$ of approximately 50% over time. On the other hand, NO_2^- selectivity continuously decreased with time. This indicates a sequential nature of the reaction with the initial formation of nitrites from nitrates hydrogenation and then the subsequent reduction of nitrites to N_2 and NH_4^+. This hypothesis is strengthened by the low FE(N_2) in the batch operation configuration, of around 2% (not

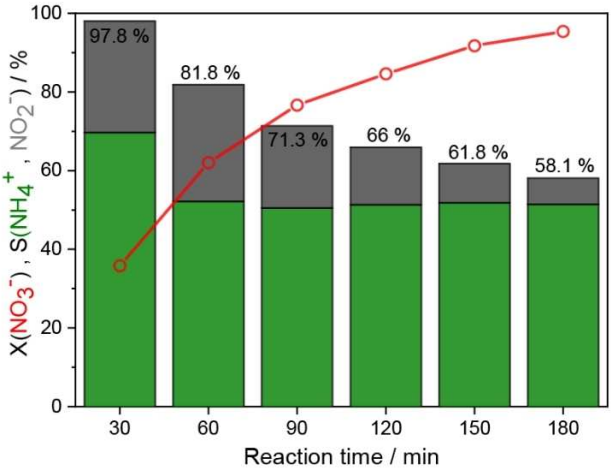

Figure 6. Nitrate conversion (red line), product selectivity [NO_2^- (grey bar) and NH_4^+ (green bar)], and pH change (blue line) in the electro-batch operation of nitrate reduction over 3 h with 40 wt% PdCu/SnO_2 at 80 °C, 20 mL cathode reservoir with $C_0(NO_3^-)$ = 100 ppm. The values shown on top of the bar are the total selectivity towards the undesired products.

shown). Due to high $S(NH_4^+)$ under chosen reaction conditions, we investigated whether CO_2 buffering of the reaction reservoir might aid in mitigating this issue (results not shown). CO_2 buffering is known to be beneficial, particularly for suppressing nitrite formation.[39,40] $S(NH_4^+)$ was not positively affected by this approach. The value was almost constant throughout the reaction run (≈60%). The nitrate conversion rate was higher with pH buffering (pH≈8) and the conversion was almost complete (≈99%) after 120 min of reaction. The observations with CO_2 addition, namely, nitrite suppression and enhanced ammonium ion formation, agree with the trends reported in the literature.[21,22]

The electro-batch operation at mild conditions allowed us to reach the maximum level of nitrate conversion, at the same time exhibiting the drawback of poor selectivity towards nitrogen [$S(N_2) < 50\%$], and ammonium as dominant reaction product formation. The high selectivity towards ammonium at low constant current (and consequently low cell potential) can be due to a different reaction pathway at these conditions. The product selectivity in the electrochemical reduction of nitrate is dependent on the applied potential at the working electrode. It is therefore possible that at low cell potentials (1.6–1.8 V), the nitrate reduction follows an electrochemical pathway, and the main reaction product is ammonium [Eq. (4)].

$$NO_3^- + 10H^+ + 8e^- \rightarrow NH_4^+ + 3H_2O \quad (4)$$

Therefore, the strategy as it is cannot be used for purification of drinking water. However, such approach could be used to produce concentrated ammonium solutions, such as those required in selective catalytic reduction (SCR) in the automotive industry or for the production of gaseous ammonia.

Photocatalytic ammonium oxidation

The above section shows that high selectivity to NH_4^+ is the bottleneck in selective reduction of nitrates to nitrogen. A literature survey indicated that NH_4^+ conversion to N_2 can be carried out by oxidation reactions, either catalytic, electrocatalytic, or photocatalytic.[41–48] We evaluated these paths to abate the formed NH_4^+ during nitrate reduction, instead of suppressing its formation. We first investigated an electrocatalytic oxidation strategy at the anode of the PEM cell (Figure 2A) by passing the effluent stream from the cathode to the anode. Despite the simplicity of the approach, performing both nitrate reduction and ammonium/nitrite abatement in one cell, a prominent deactivation was observed over time due to the blockage of the Nafion membrane by the metal cations present in water, through competitive transport with H^+.

Hence, the strategy we studied further was the photocatalytic oxidation approach (Figure 2C), for its promising activity and its greener nature, by making use of light for activation.[46–48] Metal-doped TiO_2 is known to enhance NH_4^+ conversion to N_2.[48] In this work, photo-deposited Pt/P25 (P25 is a well-known TiO_2 containing both anatase and rutile phases which shows high photocatalytic activity) was used.[49,50] Bare

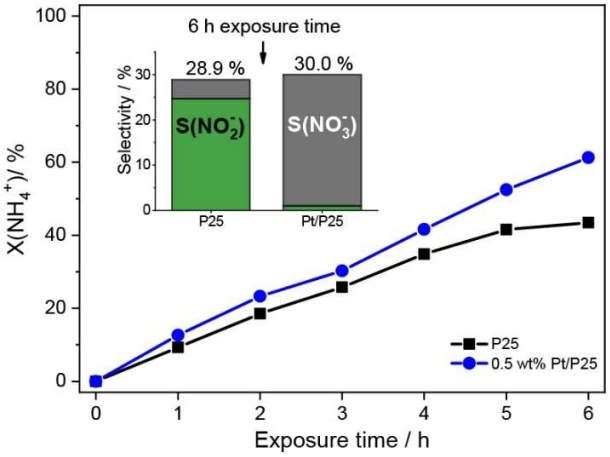

Figure 7. Ammonium ion photo-oxidation study showing $X(NH_4^+)$ versus UV-light exposure time at 20 °C and $C_0(NH_4^+) = 1000$ ppm for 0.5 wt% Pt/P25 and P25. (Inset) Product selectivity after 6 h of UV exposure. The values shown on top of the bars are $S(NO_x^-)$.

P25 has also been reported for its capabilities to convert NH_4^+ to NO_3^- and NO_2^-.[46,48] Figure 7 shows a performance comparison between P25 and Pt/P25 in terms of $X(NH_4^+)$ and $S(N_2)$ during 6 h of photo-oxidation under UV radiation at room temperature. To contrast the catalytic performance better, a solution with higher initial ammonium concentration [$C_0(NH_4^+) = 1000$ ppm, pH≈11] was used. The NH_4^+ conversion profiles (Figure 7) clearly show that the photocatalytic reaction took place over both materials. As expected, Pt/P25 (blue line) showed better photocatalytic activity for ammonium conversion (≈60%) than bare P25 (≈40%, black line).

While the conversion level was relatively similar, the product selectivity was very different for the two catalysts. Both materials achieved similar total selectivity towards nitrogen oxide ions [$S(NO_x^-) = S(NO_2^-) + S(NO_3^-)$]. Assuming $S(N_2) = 100\% - S(NO_x^-)$, the $S(N_2)$ was approximately 70% for both materials after 6 h (Figure 7, inset). For P25, nitrite was the dominant [$S(NO_2^-) = 24\%$] side products, For Pt/P25, nitrate formation was dominant [$S(NO_3^-) = 28\%$] (Figure 7, inset). This evidences that the presence of Pt on P25 promoted the secondary oxidation of nitrites to nitrates, which was confirmed from the temporal evolution of the ion concentrations (not shown). The resulting concentration of nitrates is rather high after the reaction, but this is in principle less critical than high concentrations of nitrite and ammonium ions after the reaction because of stricter regulations regarding the latter, as discussed in previous sections.

After confirming the feasibility of photocatalytic oxidation for NH_4^+ abatement, this approach was tested on the effluent solution from the cathode compartment of the PEM cell, after electrolysis-assisted nitrate reduction. Only the 0.5 wt% Pt/P25 photocatalyst was tested due to its superior performance compared to P25. The effluent solution containing approximately 8 ppm NH_4^+ (pH≈9) was tested under the same conditions (6 h, 20 °C, stirring, 100 W UV lamp). However, at 20 °C almost negligible $X(NH_4^+)$ was observed (<4%). At an

increased temperature of 50 °C, $X(NH_4^+)$ enhanced to some extent, reaching approximately 30% after 6 h. Thus, we concluded that the strategy is not as effective when the concentration of ammonium ion is low, and thus prevents decreasing the ammonium ion concentration down to the desired value (< 0.5 ppm).

Combined electro-photo approach

After reaching the limit of the approaches tested above, we further evaluated possible ideas on how to deal with nitrate, nitrite and most importantly ammonium ions. Since the sequential abatement of the nitrogen containing ions, described in the previous section, was not effective, we developed a reactor which combines the electrolysis-assisted nitrate hydrogenation in electro-batch mode with the photocatalytic ammonium oxidation in the cathode compartment (Figure 2D). This combination was made possible by covering the cathode reservoir with a UV light transparent window. Compared to the sequential abatement strategy, this combined approach may drive the overall reaction towards N_2 more effectively because all nitrogen-containing ions are not in their resting state during operation, as illustrated in Scheme 1.

The results were prominent and encouraging. After 8 h of batch operation under combined photo-electro conditions with $PdCu/SnO_2$ as nitrate reduction cathode catalyst and Pt/P25 as ammonium and nitrite oxidation photocatalyst, $X(NO_3^-)$ reached 97%, $S(NO_2^-)$ was 0.6%, and $S(NH_4^+)$ was 2.0%, with final concentrations for NO_3^-, NO_2^-, and NH_4^+ of approximately 2.4, 0.6, and 0.5 ppm, respectively. These values are almost at the aim level of this research (maximum limit for drinking water: 50, 0.5, and 0.5 ppm for NO_3^-, NO_2^-, and NH_4^+, respectively). A longer reaction time would expectedly achieve lowering these concentrations. Notably, the issue of high NH_4^+ concentration observed in the electro-batch configuration was effectively solved. Some technical aspects, such as cathode reservoir temperature and stirring efficiency to enable suitable photocatalyst dispersion, remain as practical challenges. Further systematic investigations of the approach are required to evaluate its potential application in practice. Nevertheless, the first proof-of-principle of the combined redox approach for selective nitrate conversion to nitrogen has been successfully demonstrated.

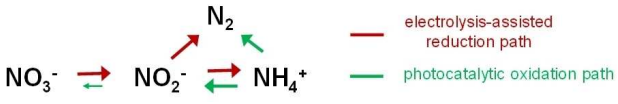

Scheme 1. Combined electrolysis-assisted reduction and photocatalytic oxidation to drive the overall reaction from nitrate ion to nitrogen selectively.

Conclusion

The feasibility of proton exchange membrane (PEM) electrolysis-assisted hydrogenation for aqueous nitrate abatement under continuous and batch operations was demonstrated and later investigated in detail to understand how conversion of nitrate ions and product selectivity are defined. Among supported metal catalysts with 40 wt% metal loading (Pt, Pd, Cu, and PdCu) over high surface area SnO_2, 40 wt% PdCu was identified as the best-performing catalyst, showing high nitrate conversion (97%) and high selectivity to N_2 (96%) in a continuous operation mode. The synergistic effects of Pd and Cu in PdCu catalyst, well documented in catalytic hydrogenation, hold for the electrolysis-assisted nitrate reduction. Based on the solution pH change during the reaction and considering the low faradaic efficiency towards nitrogen-containing reaction products, nitrate reduction likely takes place via electrolysis-assisted catalytic hydrogenation of NO_3^- by H_2, the latter being evolved electrochemically on the cathode surface. Different modes of operation such as constant cell voltage, constant current with/without recirculation, and catalytic hydrogenation were evaluated. The characteristics of the reactivity and its trends were clarified. It is possible to convert nitrates at low cell voltage (1.8 V) and at low current density; however, the high selectivity to undesired products (NO_2^- and NH_4^+, especially the latter) was found to be the major problem of the electrolysis-assisted hydrogenation of nitrates. In this work, we effectively solved this problem by introducing a photocatalytic oxidation process in the same PEM electrolyzer, namely combining electrolysis-assisted hydrogenation of nitrates and photocatalytic oxidation of ammonium and nitrite ions. The combined reaction was operated in the batch mode where a photocatalyst was suspended in the solution. Using Pt supported on TiO_2 (P25) as photocatalyst and $PdCu/SnO_2$ as cathode catalyst, we could achieve the targeted low level of contaminants concentration. This work shows new directions and approaches for water denitrification and ammonium ion abatement. The electrolysis-assisted and combined approaches were shown to be extremely powerful because of their high flexibility and no need of an external hydrogen source. The simultaneous incorporation of an oxidation process as an effective NH_4^+ mitigation strategy in nitrate reduction process is therefore proved as effective and promising.

Experimental Section

Support preparation

High-surface-area tin(IV) oxide [Brunauer-Emmett-Teller (BET) surface area of $\approx 230\ m^2 g^{-1}$, cassiterite crystal structure], synthesized by urea (CH_4N_2O, Sigma-Aldrich) precipitation methodology, was used as a support to enhance the metal dispersion over SnO_2.[51] SnO_2 was chosen as the support for its semiconductor properties, as well as its durability under harsh operating conditions (e.g., pH and electric current).[52] An aqueous solution of 0.1 M $SnCl_4$ and 10-fold excess of urea was refluxed at 90 °C for 15 h in a round-bottom

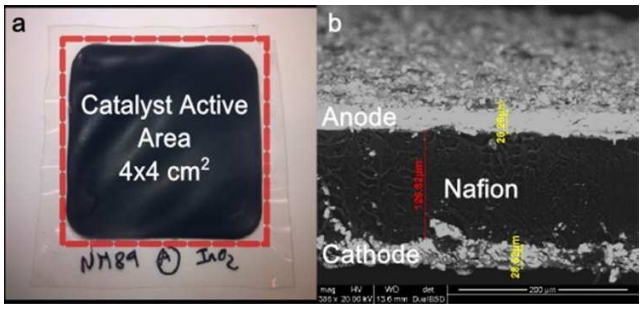

Figure 8. MEA made by spray deposition and CCM method. (a) Image taken right after catalyst deposition (fresh membrane). (b) ESEM image of the cross-section of same MEA (in red Nafion 117 membrane thickness, in yellow thickness of catalyst layers).

flask. The precipitate was isolated and washed by centrifugation, dried at 120 °C for 16 h, and calcined at 200 °C for 4 h in air.

Catalyst preparation

An ultrasound-assisted metal deposition method was employed as catalyst synthesis method. The synthesis was performed as follows. (1) The catalyst support, together with the metal [Pt, Pd, Cu, and PdCu (4:1, weight ratio)] precursor aqueous solution were mixed in a round-bottom flask and stirred for 10 min. (2) The flask was placed in an ultrasonic bath where reduction of target metal precursor(s) was performed by stepwise $NaBH_4$ (sodium borohydride, >97%, 10–40 mesh granules, Alfa Aesar) addition, after which the flask was left for 1 h under continuous sonication. (3) The powder was filtered using a vacuum funnel, (4) cleaned with excess milliQ H_2O (10:1 volume ratio of water compared to the metal precursor solution used for synthesis) for thorough Na^+ removal, and (5) dried at 100 °C for 12 h in the oven.[53] Consistent sonication is important for homogeneous metal deposition, by maximizing the contact between metal precursor and support particles. Using this procedure, we were able to avoid the formation of metal oxides, and thus no calcination and further reduction were required. At the same time, high metal surface area ($m^2\,g^{-1}_{sample}$) and thus degree of metal dispersion over the support were achieved. Pt metal dispersion as the representative case was determined by means of pulse chemisorption, in which the amount of H_2 adsorbed over Pt surface is determined. The metal dispersion was 72% and the metal surface for catalytic processes was estimated to be approximately 20 $m^2\,Pt\,g^{-1}_{sample}$. Such high Pt dispersion justified the use of the sonication $NaBH_4$ method to prepare other SnO_2-supported metal catalysts used in this study.

MEA preparation

Nafion 117 membrane (175 μm thick, Ion Power) was used as proton transport solid electrolyte. Prior to use, the membranes were treated by washing in 5 vol% H_2O_2 aqueous solution for 1 h at 80 °C to eliminate residual organic impurities, then in 0.5 M sulfuric acid for 1 h at 80 °C to incorporate water molecules and to activate the membrane by hydration.[54–56] The membrane was further treated with boiling water for 1 h in order to remove possible impurities remaining from previous treatments. The treated membranes were stored in water at ambient temperature prior to deposition of the catalyst.

Catalyst inks were made of a mixture of catalyst powder, isopropanol (4 mL) and 15.4 wt % Nafion ionomer (Nafion D-521

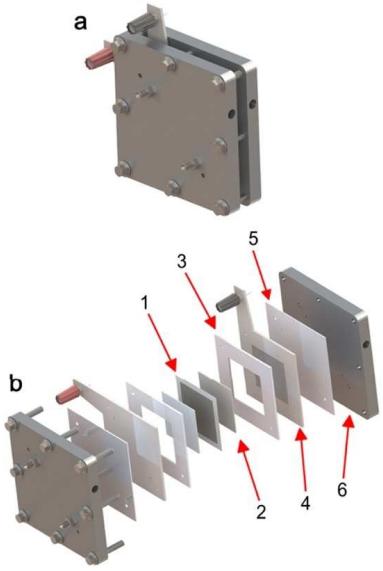

Figure 9. Flow-through PEM electrocatalytic reactor for water electrolysis and electrolysis-assisted reactions. (a) Fully assembled cell and (b) layer-by-layer reactor components: (1) MEA, (2) gas diffusion layer (GDL), (3) PTFE gasket, (4) current collector, (5) PTFE back gasket, and (6) front or end plate.

dispersion, 5 wt% in water and 1-propanol, ≥0.92 meq g^{-1} exchange capacity, Alfa Aesar) of dry catalyst amount. The ink was sonicated for 1 h in an ultrasound bath. As the methodology to produce our MEA we chose the spray deposition method.[57,58] The deposition procedure was as follows: catalyst-containing inks were coated over the Nafion membrane (active area of 4×4 cm^2) by using an airbrush ($Ø_{nozzle}$: 0.5 mm, Ventus Titan) and fixing the Nafion membrane in a heated holder with an open window. The deposition temperature was set at 85 °C to evaporate the solvent during the deposition, avoiding membrane swelling. Homogeneous and uniform catalyst layers on both sides of Nafion membrane (Figure 8) were achieved reproducibly. An example of a ready-to-be-tested MEA is shown on Figure 8a. The thickness of the catalyst layer over the membrane was measured by means of environmental scanning electron microscopy (ESEM) using a FEI Quanta 600 microscope [equipped with energy-dispersive X-ray spectroscope (EDX) from Oxford Systems] by focusing the electron beam towards the cross section of the MEA (Figure 8b). The thickness of catalyst layers at both anode and cathode side was ca. 25 μm.

PEM cell

The assembly of the PEM cell is represented in Figure 9a, and its layer-by-layer components are shown in Figure 9b. A PEM cell is based on a multilayer arrangement where the most important parts are: (1) MEA, (2) gas diffusion layers, and (4) current collectors with serpentine flow fields. In our design, we made use of (1) MEAs described before, (2) porous sintered titanium gas diffusion layers (GDL, 4×4 cm^2, 1 mm thickness, pore size 50 μm, Xinxiang Filter Technology Co.), and (4) Ti current collectors (2 mm thickness) with machined flow fields (1 cm^3 total channel volume, with single serpentine groove). Grade 1 titanium was used as material of choice, to avoid corrosion of (2) and (4). MEA and GDL were sandwiched between the current collectors, which were held together by 8 screws through the aluminum cell housing plates (1 cm thickness). Sealing and electrode insulation were provided by PTFE gaskets (3, 5). Screw torque was set at 5 N·m, providing a leak-

free system and achieving reproducible testing conditions. Electrical connectors were plugged to the current collector plates through connection pins shown in Figure 9 (red and black for anode (+) and cathode (−), respectively). The PEM cell was first integrated in a flow system and modified further to carry out different reduction (NO_3^-), mitigation (NH_4^+), and red-ox (NO_3^-–NH_4^+) strategies (Figure 2).

Continuous electrolysis-assisted nitrate reduction

Electrolysis-assisted nitrate reduction experiments were performed using the PEM cell in Figure 9. Figure 2A shows a layout of the reaction cell and flow system configuration. The nitrate solution reservoir and the auxiliary peristaltic pump were added as main features compared to a typical PEM water electrolysis system. The pH of the cathode effluent stream was continuously measured with a Crison pH meter (model 5028, probe Ø = 3 mm). Peristaltic pumps (Reglo Digital, 2 channels; Ismatec) were used to feed milliQ H_2O and nitrate solution to the PEM cell. The working temperature and flow rate of nitrate solution were set at 80 °C, and 160 μL min^{-1}, respectively. Pure water was passed through the anode compartment at a flow rate of 0.5 mL min^{-1}. All NO_3^- reduction tests were evaluated using a C_0 = 100 ppm NO_3^- solution prepared from $NaNO_3$. MEA layer-by-layer composition for all NO_3^- reduction tests was IrO_2 | Nafion | 40 wt% M/SnO_2; where M=Pt, Pd, Cu, and PdCu (4:1). A potentiostat (BioLogic SP-150) was used as an external power source with fine *V–I* control. For high-potential measurements (≈2.1–2.7 V), a combination of the potentiostat and a booster (BioLogic VMP3B-5, 5 A/20 V) was used. Automated and programmable sample collection was done by using an in-house built autosampler.

Low-potential electrolysis-assisted batch operation configuration

The flow-through cathode compartment was replaced by a batch cell compartment made of aluminum, with a 20 mL solution reservoir. In the batch operation mode, the reactor was placed in a horizontal position (Figure 2B). Water flow rate in the anode compartment was kept same as in the flow-through experiments (0.5 mL min^{-1}). The solution in the cathode compartment was stirred to enhance mass transfer and solution homogeneity.

Photocatalytic ammonium oxidation

Commercial P25 Titania (TiO_2, Degussa) was used as catalyst for ammonium and nitrite photo-oxidation. Besides P25, photo-deposited 0.5 wt% Pt/P25 was also tested. A round-bottom flask equipped with a cooling jacket for temperature control was used as a batch photo-reactor (Figure 2C) with catalyst concentration of 3 g L^{-1} and operated under vigorous stirring. The light source was a UV-curing 100 W high-pressure Hg lamp (Handy Cure HLR400T-1, Senlight Corp. with a nominal UV light intensity of 170 mW cm^{-2}). A circular UV fused silica window (EKSMA OPTICS, 1 cm thickness) was placed on top of the reactor to avoid evaporation of the solution.

Combined electrolysis-assisted reduction and photocatalytic oxidation

A square UV fused silica window (1 cm thickness) was placed on top of the cathode reservoir of the PEM cell to avoid evaporation of the nitrate solution. The MEA composition was similar to that used in flow-through and batch experiments, using 40 wt% PdCu/SnO_2 as cathode material. Photocatalysts (0.5 wt% Pt/P25 and P25) were suspended in the cathode reservoir and stirred during reaction (Figure 2D). The same UV light source as in previous experiments was used.

Analytical system

An ion chromatograph (883-IC Basic, Metrohm AG, Switzerland) was used for the quantification of ions (NO_3^-, NO_2^-, and NH_4^+). Metrosep A Supp 4 (250/4.0) and Metrosep C6 (250/4.0) separation columns were used for separation of anions and cations, respectively. The liquid samples were filtered using Nylon syringe filters (0.45 μm pore size, FilterLab) before injection into the 20 μL sample loop of the IC. All concentration values have been corrected taking in account the dilution effect at the cathode due to electro-osmotic water drag.[59–61]

MS (Pfeiffer Vacuum, Omnistar GSD 320) was used to analyze gaseous nitrate reduction products. The reactor outlet gas flow was fed to the MS after drying by means of a gas–liquid separator, to remove water vapor. The monitored gas species were: N_2 (m/z = 28, 14), H_2 (m/z = 2), N_2O (m/z = 44, 30), NO (m/z = 30, 14), NH_3 (m/z = 17, 16) and NH_2OH (m/z = 33, 32, 16).

Acknowledgements

Financial support from the ICIQ foundation and MINECO (CTQ2012-34153 and CTQ2016-75499-R (FEDER-UE)) is greatly acknowledged.

Conflict of Interest

The authors declare no conflict of interest.

Keywords: hydrogenation · nitrate removal · oxidation · PEM electrolysis · photocatalysis

[1] J. N. Galloway, A. R. Townsend, J. W. Erisman, M. Bekunda, Z. Cai, J. R. Freney, L. A. Martinelli, S. P. Seitzinger, M. A. Sutton, *Science* **2008**, *320*, 889–892.
[2] Council of the European Union, *Official Journal of the European Communities: Legislation* **1991**, *34*, L375.
[3] Environmental Protection Agency, *National primary drinking water regulations, Vol. 40*, **1998**.
[4] World Health Organization, *Guidelines for drinking-water quality, 4th edition, incorporating the 1st addendum*, **2017**.
[5] Council of the European Union, Official Journal of the *European Communities: Legislation* **1998**, *41*, L330.
[6] V. Jensen, J. Darby, C. Seidel, C. Gorman, *Drinking water treatment for nitrate, Vol. 6*, **2012**.
[7] S. Hörold, K. D. Vorlop, T. Tacke, M. Sell, *Catal. Today* **1993**, *17*, 21–30.
[8] A. Pintar, J. Batista, J. Levec, T. Kajiuchi, *Appl. Catal. B* **1996**, *11*, 81–98.
[9] F. Deganello, L. F. Liotta, A. Macaluso, A. M. Venezia, G. Deganello, *Appl. Catal. B* **2000**, *24*, 265–273.
[10] Y. Yoshinaga, T. Akita, I. Mikami, T. Okuhara, *J. Catal.* **2002**, *207*, 37–45.
[11] N. Barrabés, J. Just, A. Dafinov, F. Medina, J. L. G. Fierro, J. E. Sueiras, P. Salagre, Y. Cesteros, *Appl. Catal. B* **2006**, *62*, 77–85.
[12] X. Huo, D. J. Van Hoomissen, J. Liu, S. Vyas, T. J. Strathmann, *Appl. Catal. B* **2017**, *211*, 188–198.
[13] N. Barrabés, J. Sá, *Appl. Catal. B* **2011**, *104*, 1–5.
[14] V. Rosca, M. Duca, M. T. de Groot, M. T. M. Koper, *Chem. Rev.* **2009**, *109*, 2209–2244.

[15] K. Bouzek, M. Paidar, A. Sadílková, H. Bergmann, *J. Appl. Electrochem.* **2001**, *31*, 1185–1193.
[16] O. Brylev, M. Sarrazin, L. Roué, D. Bélanger, *Electrochim. Acta* **2007**, *52*, 6237–6247.
[17] S. Taguchi, J. M. Feliu, *Electrochim. Acta* **2007**, *52*, 6023–6033.
[18] M. Li, C. Feng, Z. Zhang, N. Sugiura, *Electrochim. Acta* **2009**, *54*, 4600–4606.
[19] M. Li, C. Feng, Z. Zhang, Z. Shen, N. Sugiura, *Electrochem. Commun.* **2009**, *11*, 1853–1856.
[20] M. Duca, M. T. Koper, *Energy Environ. Sci.* **2012**, *5*, 9726–9742.
[21] M. Machida, K. Sato, I. Ishibashi, M. A. Hasnat, K. Ikeue, *Chem. Commun.* **2006**, 732–734.
[22] M. A. Hasnat, I. Ishibashi, K. Sato, R. Agui, T. Yamaguchi, K. Ikeue, M. Machida, *Bull. Chem. Soc. Jpn.* **2008**, *81*, 1675–1680.
[23] M. Hasnat, M. Karim, M. Machida, *Catal. Commun.* **2009**, *10*, 1975–1979.
[24] M. Hasnat, M. S. Alam, M. M.-U. Karim, M. Rashed, M. Machida, *Appl. Catal. B* **2011**, *107*, 294–301.
[25] M. A. Hasnat, N. Ahamad, S. M. Nizam Uddin, N. Mohamed, *Appl. Surf. Sci.* **2012**, *258*, 3309–3314.
[26] H. Cheng, K. Scott, P. A. Christensen, *Chem. Eng. J.* **2005**, *108*, 257–268.
[27] L. Szpyrkowicz, S. Daniele, M. Radaelli, S. Specchia, *Appl. Catal. B* **2006**, *66*, 40–50.
[28] R. Abdallah, F. Geneste, T. Labasque, H. Djelal, F. Fourcade, A. Amrane, S. Taha, D. Floner, *J. Electroanal. Chem.* **2014**, *727*, 148–153.
[29] P. Kuang, K. Natsui, Y. Einaga, *Chemosphere* **2018**, *210*, 524–530.
[30] Y. Wang, A. Xu, Z. Wang, L. Huang, J. Li, F. Li, J. Wicks, M. Luo, D.-H. Nam, C.-S. Tan, Y. Ding, J. Wu, Y. Lum, C.-T. Dinh, D. Sinton, G. Zheng, E. H. Sargent, *J. Am. Chem. Soc.* **2020**, *142*, 5702–5708.
[31] J. M. McEnaney, S. J. Blair, A. C. Nielander, J. A. Schwalbe, D. M. Koshy, M. Cargnello, T. F. Jaramillo, *ACS Sustainable Chem. Eng.* **2020**, *8*, 2672–2681.
[32] T. Corrales-Sánchez, J. Ampurdanés, A. Urakawa, *Int. J. Hydrogen Energy* **2014**, *39*, 20837–20843.
[33] J. Ampurdanés, M. Chourashiya, A. Urakawa, *Catal. Today* **2019**, *336*, 161–168.
[34] N. I. Kolev, in *Multiphase Flow Dynamics 4: Turbulence, Gas Adsorption and Release, Diesel Fuel Properties* (Ed.: N. I. Kolev), Springer, Berlin, Heidelberg, **2012**, pp. 209–239.
[35] C. G. Vayenas, S. Bebelis, S. Neophytides, *J. Phys. Chem.* **1988**, *92*, 5083–5085.
[36] C. Vayenas, S. Brosda, C. Pliangos, *J. Catal.* **2001**, *203*, 329–350.
[37] A. Katsaounis, *J. Appl. Electrochem.* **2010**, *40*, 885–902.
[38] M. Hasnat, R. Agui, S. Hinokuma, T. Yamaguchi, M. Machida, *Catal. Commun.* **2009**, *10*, 1132–1135.
[39] M. D'Arino, F. Pinna, G. Strukul, *Appl. Catal. B* **2004**, *53*, 161–168.
[40] R. Gavagnin, L. Biasetto, F. Pinna, G. Strukul, *Appl. Catal. B* **2002**, *38*, 91–99.
[41] M. Baerns, R. Imbihl, V. Kondratenko, R. Kraehnert, W. Offermans, R. Van Santen, A. Scheibe, *J. Catal.* **2005**, *232*, 226–238.
[42] R. Imbihl, A. Scheibe, Y. Zeng, S. Günther, R. Kraehnert, V. Kondratenko, M. Baerns, W. Offermans, A. Jansen, R. Van Santen, *Phys. Chem. Chem. Phys.* **2007**, *9*, 3522–3540.
[43] L. Li, Y. Liu, *J. Hazard. Mater.* **2009**, *161*, 1010–1016.
[44] N. J. Bunce, D. Bejan, *Electrochim. Acta* **2011**, *56*, 8085–8093.
[45] L. Candido, J. A. C. Ponciano Gomes, *Mater. Chem. Phys.* **2011**, *129*, 1146–1151.
[46] X. D. Zhu, S. R. Castleberry, M. A. Nanny, E. C. Butler, *Environ. Sci. Technol.* **2005**, *39*, 3784–3791.
[47] J. Nemoto, N. Gokan, H. Ueno, M. Kaneko, *J. Photochem. Photobiol. A* **2007**, *185*, 295–300.
[48] M. A. Al Sawah, D. Richard, C. De Bellefon, J.-M. Chovelon, C. Ferronato, *C. R. Chim.* **2010**, *13*, 502–507.
[49] R. I. Bickley, T. Gonzalez-Carreno, J. S. Lees, L. Palmisano, R. J. D. Tilley, *J. Solid State Chem.* **1991**, *92*, 178–190.
[50] D. C. Hurum, A. G. Agrios, K. A. Gray, T. Rajh, M. C. Thurnauer, *J. Phys. Chem. B* **2003**, *107*, 4545–4549.
[51] A. Hagemeyer, Z. Hogan, M. Schlichter, B. Smaka, G. Streukens, H. Turner, A. Volpe, H. Weinberg, K. Yaccato, *Appl. Catal. A* **2007**, *317*, 139–148.
[52] K. Sasaki, F. Takasaki, Z. Noda, S. Hayashi, Y. Shiratori, K. Ito, *ECS Trans.* **2010**, *33*, 473–482.
[53] O. Ilinich, F. P. Cuperus, R. Van Gemert, E. Gribov, L. Nosova, *Sep. Purif. Technol.* **2000**, *21*, 55–60.
[54] C. Yang, P. Costamagna, S. Srinivasan, J. Benziger, A. Bocarsly, *J. Power Sources* **2001**, *103*, 1–9.
[55] S. Lee, S. Mukerjee, J. McBreen, Y. Rho, Y. Kho, T. Lee, *Electrochim. Acta* **1998**, *43*, 3693–3701.
[56] Z. Lu, G. Polizos, D. D. Macdonald, E. Manias, *J. Electrochem. Soc.* **2008**, *155*, B163-B171.
[57] L. Sun, R. Ran, Z. Shao, *Int. J. Hydrogen Energy* **2010**, *35*, 2921–2925.
[58] L. Sun, R. Ran, G. Wang, Z. Shao, *Solid State Ionics* **2008**, *179*, 960–965.
[59] X. M. Ren, S. Gottesfeld, *J. Electrochem. Soc.* **2001**, *148*, A87-A93.
[60] T. A. Zawodzinski, J. Davey, J. Valerio, S. Gottesfeld, *Electrochim. Acta* **1995**, *40*, 297–302.
[61] T. A. Zawodzinski, C. Derouin, S. Radzinski, R. J. Sherman, V. T. Smith, T. E. Springer, S. Gottesfeld, *J. Electrochem. Soc.* **1993**, *140*, 1041–1047.

Manuscript received: December 8, 2020
Revised manuscript received: December 30, 2020
Accepted manuscript online: December 30, 2020
Version of record online: ■■, ■■■

FULL PAPERS

Synergistic combination: Electrolysis-assisted nitrate hydrogenation enabled by the cathode catalyst of a polymeric electrolyte membrane (PEM) cell can efficiently convert nitrate to N_2, but it suffers from product selectivity and forms toxic by-products (NO_2^- and NH_4^+). Simultaneous photocatalytic oxidation affords drastic removal of these toxic by-products and guides the overall reaction towards N_2 formation.

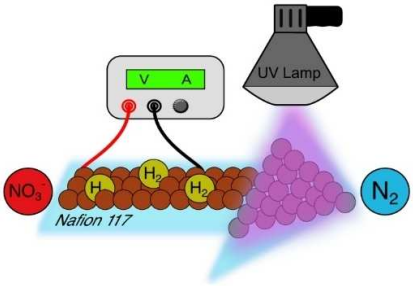

*Dr. J. Ampurdanés, S. Bunea, Prof. A. Urakawa**

1 – 12

PEM Electrolysis-Assisted Catalysis Combined with Photocatalytic Oxidation towards Complete Abatement of Nitrogen-Containing Contaminants in Water